Shell-model description of lattice dynamical properties of $MgH_2$



2005 J. Phys.: Condens. Matter 17 7133

(http://iopscience.iop.org/0953-8984/17/44/006)

INSTITUTE OF PHYSICS PUBLISHING JOURNAL OF PHYSICS: CONDENSED MATTER

J. Phys.: Condens. Matter **17** (2005) 7133–7141 doi:10.1088/0953-8984/17/44/006

# Shell-model description of lattice dynamical properties of $MgH_2$

**J Lasave, F Dominguez, S Koval[1], M G Stachiotti and R L Migoni**

Instituto de Física Rosario, Universidad Nacional de Rosario, 27 de Febrero 210 Bis, 2000 Rosario, Argentina

E-mail: koval@ifir.edu.ar

Received 11 August 2005
Published 18 October 2005
Online at stacks.iop.org/JPhysCM/17/7133

**Abstract**

We develop a shell model (SM) for magnesium hydride with interatomic potentials and anisotropic core–shell interactions. The model is fitted to measured Raman modes and *ab initio* results that we obtain for the phonons at the Γ point. We achieve a very good agreement for the Raman and silent phonons, while the infrared-active modes are less accurately described. Using the developed SM, we have computed the phonon dispersion throughout the Brillouin zone (BZ), which turns out to be in very good agreement with previous first-principles results. The SM partial phonon density of states due to hydrogen shows very good agreement with the experimental one. The temperature dependence of the specific heat is also calculated and shows good accordance with measurements.

## 1. Introduction

Metal hydrides have been widely studied in the past for fundamental interest, as well as for various applications. They are potential candidates as energy storing compounds, and many of them show superconductivity if they are doped to become metallic [1]. In particular, magnesium hydride ($MgH_2$) has been considered to be used as a hydrogen storage medium, due to its large weight percentage of hydrogen in the compound. However, $MgH_2$ is thermodynamically very stable, and the dissociation reaction has a slow rate, precluding its application for H storage. Therefore, understanding of its microscopic properties is essential to improve its dehydrogenation performance.

Several *ab initio* calculations were carried out in the past years with the aim to understand the electronic properties and their relationship with the stability of several hydrides [2–5]. Very recently, a linear response calculation based on the density functional perturbation theory was carried out for $MgH_2$, and the phonon dispersion curves along the symmetry directions were

[1] Author to whom any correspondence should be addressed.

obtained [6]. They calculated atomic displacement parameters, crystal structure factors, and charge density distributions at finite temperature and made a comparison of the obtained results with available experimental data. However, this kind of approach is not feasible when dealing with large scale dynamical calculations, as for example, molecular dynamics simulations at finite temperature. In this case, it is necessary to determine reliable potential parameters between atoms from phenomenological modelizations, that will then be used in the large scale simulations.

The purpose of this study is to obtain a reliable model of $MgH_2$, which can account for different integral phonon properties measured in this system. In order to achieve this objective, we first performed *ab initio* calculations with the linear augmented plane-wave (LAPW) method to determine the zone centre phonons of $MgH_2$. We then built a shell model which reproduces the *ab initio* results and the available Raman data at the BZ centre and we used it to calculate the phonons throughout the entire BZ. The phonon dispersions in different symmetry directions of the BZ were also compared with recent linear response *ab initio* calculations. The total and partial hydrogen phonon density of states and the specific heat were computed and compared to the experimental data.

The paper is organized as follows: in section 2 we explain the *ab initio* method and give details of the first principles calculations. Details of the shell model used and the model calculations are presented in section 3. In section 4 we analyse and discuss the results obtained and their comparison to the experiment. Finally, in section 5 we elaborate our conclusions.

## 2. *Ab initio* calculations

The *ab initio* calculations were performed within the local density approximation (LDA) to density functional theory using the full-potential linearized augmented plane-wave (LAPW) method as implemented in the WIEN97 code [7]. In this method no shape approximation on either the potential or the electronic charge density is made. The Perdew–Burke–Ernzerhof [8] parametrization of the exchange–correlation potential was used.

Integrations in reciprocal space were performed using a $6 \times 6 \times 9$ mesh, representing 54 $\boldsymbol{k}$-points in the irreducible part of the Brillouin zone.

The atomic sphere radii 1.6 and 1.5 au were used for Mg and H, respectively. The parameter $RK_{\max}$, which controls the size of the basis sets in these calculations, was set to 7.5. This gives well converged basis sets consisting of approximately 4040 LAPW functions plus local orbitals, which are introduced in order to include in the basis set the Mg 2p and Mg 3s orbitals.

$MgH_2$ possesses the rutile type structure depicted in figure 1. It is simple tetragonal with two formula units per unit cell. The calculations are performed by fixing the lattice parameters at their experimentally determined values for normal ambient temperature and pressure: $a = 4.52$ Å in the basal plane, and $c = 3.02$ Å along the tetragonal axis [9]. The Mg–H distance $d_{\mathrm{Mg-H}}$ along the [110] direction of the basal plane is not determined by symmetry. The value we obtain from the total energy minimization is 1.95 Å, in close agreement with the experimental value of 1.96 Å [10].

The first step in order to calculate the zone-centre ($\Gamma$) phonon frequencies was to determine the irreducible basis vectors for the dynamical matrix $\mathcal{D}$ ($\Gamma$) by means of group theory analysis [11]. This procedure allows us to decompose $\mathcal{D}$ into blocks, each of them corresponding to an irreducible representation (IR) of the $\boldsymbol{q}$-group.

For those IRs which comprise several modes, the frequencies and eigenvectors are evaluated by diagonalizing the corresponding $\mathcal{D}$ block. In the case of $MgH_2$, these are exclusively infrared-active modes. For each of these phonons, the relative atom displacements

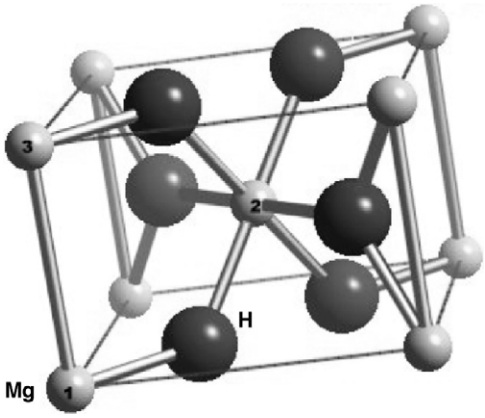


**Figure 1.** Conventional tetragonal cell of $MgH_2$.

in the primitive unit cell are obtained dividing the corresponding eigenvector by the square root of the atom masses.

The phonon frequencies and eigenvectors are determined by using the frozen phonon technique. This approach consists in imposing, for the phonons corresponding to a given IR, small atomic displacements compatible with the corresponding eigenvector form [11]. We displace the atoms from the positions corresponding to the experimental lattice parameters and the *ab initio* equilibrium value of $d_{Mg-H}$. We consider displacements smaller than 0.2% of the lattice constant $a$, which ensures linearity between forces and displacements. The calculated forces on each atom allow us then to construct the dynamical matrix block corresponding to the selected phonon symmetry. From this we obtain the relative atomic displacements corresponding to the infrared active modes of symmetry $B_{1u}$, $E_u$ and $A_{2u}$, as summarized in table 1. Not shown are the acoustic modes: a single $A_{2u}$ and a degenerate $E_u$ mode. Also, we do not show the Raman modes $A_{1g}$, $B_{1g}$, $B_{2g}$ and $E_g$ and the silent mode $A_{2g}$, whose eigenvectors are completely determined by symmetry and are given in [11].

## 3. Shell model calculations

The calculation of the phonon dispersion relations throughout the Brillouin zone of $MgH_2$ is carried out in the framework of the shell model. This takes into account short-range repulsive interactions arising from the wavefunction overlap between neighbouring ions and long-range Coulomb interactions as well as ionic polarizabilities.

In the present model, every ion is represented by an electronic shell harmonically coupled to a core. For the Mg ions, which occupy sites with inversion symmetry, each shell has the same equilibrium position as its core, and they are assumed to be isotropically coupled by a spring $K$. The negative H ions are located at sites where there is a nonzero static electric field, therefore their equilibrium core and shell positions are different. In this work, as in most shell-model calculations, these equilibrium dipoles are ignored [12], assuming the same equilibrium position for the shell and the core. As the H sites have lower symmetry, an anisotropic core–shell interaction is assumed, with components $K_\parallel$ in the plane of the nearest-neighbour Mg sites 1, 2 and 3 (see figure 1), and $K_\perp$ perpendicular to this plane.

The short-range interactions are represented by pair potentials of the Born–Mayer form: $V(r) = ae^{-br}$. These potentials are assumed to act exclusively between shells and to be rigorously zero beyond a certain distance by imposing cut-offs. First- and second-neighbour

**Table 1.** Atomic displacements relative to hydrogen and frequencies of the infrared active phonons at the Γ point.

| Atom | Component | $B_{1u}$ | | | $E_u$ | | $A_{2u}$ |
|---|---|---|---|---|---|---|---|
| $Mg_{(1)}$ | $x$ | 0 | 0 | 0 | −0.08 | 0 | 0 |
| | $y$ | 0 | 0 | 0.02 | 0 | 4.11 | 0 |
| | $z$ | −0.04 | −1.96 | 0 | 0 | 0 | 0.08 |
| $Mg_{(2)}$ | $x$ | 0 | 0 | 0 | −0.08 | 0 | 0 |
| | $y$ | 0 | 0 | −0.02 | 0 | −4.11 | 0 |
| | $z$ | 0.04 | −1.96 | 0 | 0 | 0 | 0.08 |
| $H_{(1)}$ | $x$ | 0 | 0 | 0 | 1 | 0 | 0 |
| | $y$ | 0 | 0 | 1 | 0 | −1 | 0 |
| | $z$ | −1 | 1 | 0 | 0 | 0 | −1 |
| $H_{(2)}$ | $x$ | 0 | 0 | 0 | 1 | 0 | 0 |
| | $y$ | 0 | 0 | 1 | 0 | −1 | 0 |
| | $z$ | −1 | 1 | 0 | 0 | 0 | −1 |
| $H_{(3)}$ | $x$ | 0 | 0 | 0 | 1 | 0 | 0 |
| | $y$ | 0 | 0 | −1 | 0 | 1 | 0 |
| | $z$ | 1 | −1 | 0 | 0 | 0 | −1 |
| $H_{(4)}$ | $x$ | 0 | 0 | 0 | 1 | 0 | 0 |
| | $y$ | 0 | 0 | −1 | 0 | 1 | 0 |
| | $z$ | 1 | −1 | 0 | 0 | 0 | −1 |
| | $\nu$ ($cm^{-1}$) | 1105 | 175 | 1051 | 743 | 292 | 845 |

**Table 2.** Shell model potential parameters ($a, b$), longitudinal and transversal force constants between neighbouring ions ($A$, $B$, respectively), ionic and shell charges ($Z, Y$, respectively), and on-site core–shell force constant $K$.

| Interaction | $a$ (eV) | $b$ ($Å^{-1}$) | $A$ ($e^2/v_a$) | $B$ ($e^2/v_a$) | Ion | $Z$ ($e$) | $Y$ ($e$) | $K$ ($e^2/v_a$) |
|---|---|---|---|---|---|---|---|---|
| Mg–H | 1012 | 3.9 | 33.40 | −4.40 | Mg | 1.836 | 0 | ∞ |
| H–H | 5558 | 4.12 | 12.61 | −1.21 | H | −0.918 | −1.095 | 33.62 (∥) |
| | | | | | | | | 44.4 (⊥) |

H–H interactions are included and only nearest-neighbour Mg–H interactions are considered. The Mg–Mg interactions are neglected due to the large separation between these atoms (≈3 Å).

Thus, the model contains only eight parameters. The initial values of the short-range potential parameters $a$ and $b$ were taken from a previous rigid-ion model calculation with only four parameters [13]. In that work, the potential interactions were fixed by the bulk compressibility and the equilibrium condition for the experimental values of the structural parameters. We additionally adjust the potential parameters in order to fit the available Raman [14] and *ab initio* values of the Γ-phonon frequencies. The best agreement obtained corresponds to the parameter set shown in table 2.

The Γ-phonon frequencies obtained with the shell model are compared with those resulting from the LAPW calculations and the available experimental ones from Raman measurements [14] in table 3. The LAPW frequencies are in very good agreement with the experiment. The SM results are in close agreement with the LAPW results for the Raman and silent modes, although some discrepancies are observed for the infrared active modes $B_{1u}$, $E_u$ and $A_{2u}$. Since the symmetry assignment of the phonons shown in figure 1 of [6] is not made, it is not possible to identify unambiguously the modes to compare with our results on table 3. The Raman modes, whose frequencies are expressed numerically in that paper, agree very well with our results. Also a good qualitative agreement is found for the remaining Γ-modes.

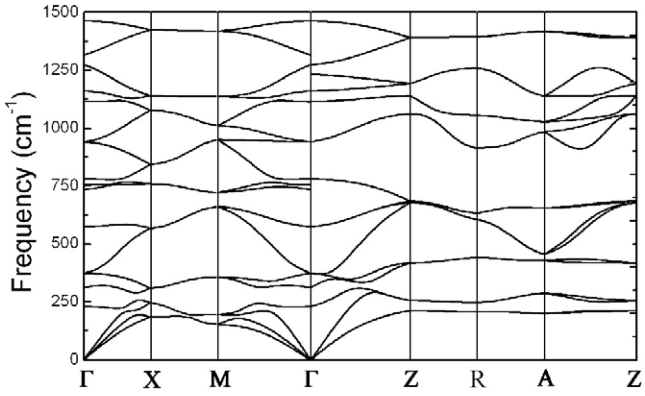


**Figure 2.** Shell-model phonon dispersion curves of $MgH_2$ along different symmetry directions in the Brillouin zone.

**Table 3.** Frequencies of the TO zone-centre modes of $MgH_2$: for the shell model, the LAPW calculation and the experiment[a] (unit: $cm^{-1}$).

| Mode | Activity | Shell model | LAPW | Experiment[a] |
|---|---|---|---|---|
| $B_{1u}$ | Infrared | 1160 | 1105 | |
| | | 230 | 175 | |
| $E_u$ | Infrared | 1114 | 1051 | |
| | | 573 | 743 | |
| | | 373 | 292 | |
| $A_{2u}$ | Infrared | 736 | 845 | |
| $B_{2g}$ | Raman | 1463 | 1461 | |
| $A_{1g}$ | | 1274 | 1277 | 1276 |
| $E_g$ | | 940 | 963 | 950 |
| $B_{1g}$ | | 312 | 289 | 300 |
| $A_{2g}$ | Silent | 780 | 787 | |

[a] Reference [14].

We use the shell model with parameters fitted to the Γ-phonon frequencies to calculate the dispersion relations in the entire Brillouin zone. The resulting dispersion curves along different symmetry directions are shown in figure 2. The phonon frequencies obtained are stable throughout the whole Brillouin zone. These curves are qualitatively in good accordance with the first-principles ones in figure 1 of [6]. There are only minor quantitative differences. The overall agreement is remarkable considering that the shell model was fitted only to the Γ-phonons.

## 4. Further results and discussion

### *4.1. Density of states (DOS)*

With the aid of the shell model developed, we calculated the total and partial phonon density of states (PDOS) projected over different atoms. In figure 3 we plot the obtained PDOS for both atoms, Mg and H. The Mg band extends on the low-frequency region from 0 to ≈450 $cm^{-1}$, while the H bands are visualized mostly on the high-frequency region, extended from ≈300

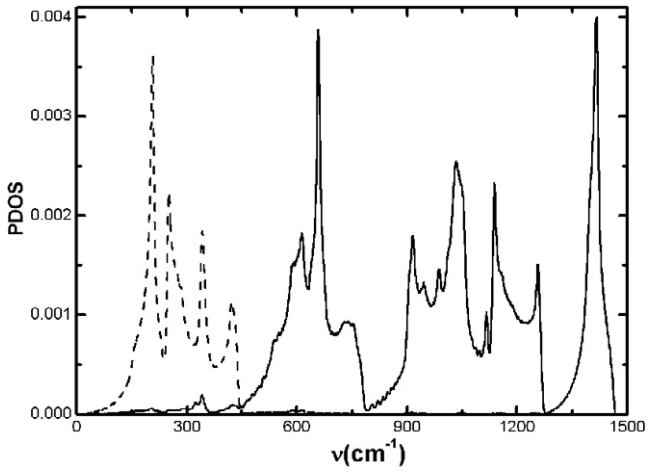


**Figure 3.** Calculated partial phonon density of states for magnesium (dashed lines) and hydrogen (solid lines). The spectra are normalized such that the area under the H-curve is equal to one.

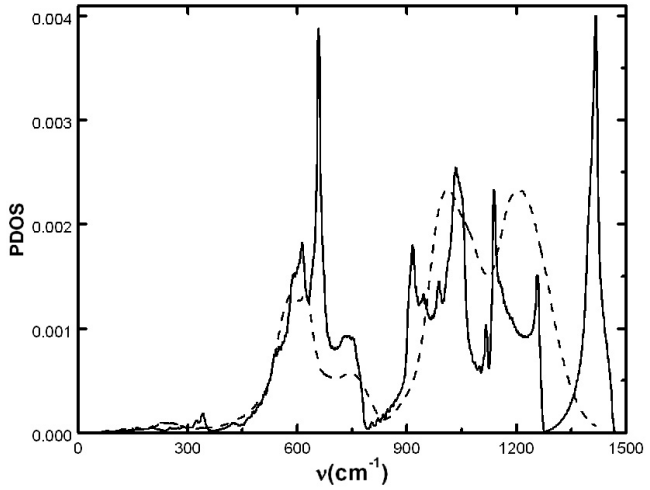


**Figure 4.** Partial phonon density of states for hydrogen derived from our SM calculations (solid lines) and the neutron scattering experiments of [14] (dashed lines). The spectra are normalized such that the area under each curve is equal to one.

to almost 1500 $cm^{-1}$. As a consequence of the large mass difference between Mg and H, and the ionic character of their bonding, both Mg and H PDOS have a very small mixture character. In the Mg bands, there is about 10 and 5% H contribution to the peaks observed at 370 and 420 $cm^{-1}$ respectively. These peaks correspond to almost dispersion-less low-lying optical bands which are hybridized with the acoustic bands near the Brillouin zone boundary in the (100) and (110) directions, as is observed in figure 2. As a consequence of the similarity between the shell-model and *ab initio* dispersion curves, the total DOSs are in remarkable agreement [6].

The results for the hydrogen PDOS are compared in figure 4 with the corresponding experimental data derived from inelastic-neutron scattering measurements [14]. Our results

show in general good agreement with the experiment. The main bands of the spectra, which are observed experimentally centred at ≈280, 600, 980 and 1200 $cm^{-1}$, are qualitatively well reproduced by the calculations. The gaps that separate the first three bands are located in our calculations at ≈400 and 800 $cm^{-1}$, in close agreement with the experimental gaps at ≈350 and 850 $cm^{-1}$ [14]. The pseudogap observed experimentally at ≈1100 $cm^{-1}$ is also reproduced in our calculations (see figure 4). Our calculations show an extra band centred at ≈1470 $cm^{-1}$, which was not observed in the neutron-scattering experiments of Santiesteban *et al* [14] due to the fact that they considered neutron energies up to 170 meV (≈1370 $cm^{-1}$). This band corresponds to the Raman active $B_{2g}$ mode, not measured but obtained both in our *ab initio* calculation and the previous one from [6].

The large widths observed in the hydrogen bands in the region between 500 and 1300 $cm^{-1}$, which should be related to the dispersion of H optic phonon branches, have been ascribed in [14] to strong H–H interactions. In fact, the H branches show in figure 2 dispersions that explain the widths of the above bands, but the H–H interactions arising from our calculations are relatively weak; hydrogens interact mainly with Mg. Our results show additional structures of the bands, which either could not be resolved in the experiments or are washed up by anharmonicities that are not considered in our model.

### *4.2. Specific heat*

Using the total DOS derived by the present shell model, we have computed the molar specific heat at constant volume with the aid of the expression

$$C_v(T) = 3nR \int_0^{\omega_{\max}} g(\omega) E\left(\frac{\hbar\omega}{k_B T}\right) \mathrm{d}\omega, \tag{1}$$

where $n$ is the number of atoms per formula unit, $R$ is the molar gas constant, $g(\omega)$ is the normalized total DOS determined by the shell model and $E(x)$ is the Einstein function:

$$E(x) = \left(\frac{x/2}{\sinh(x/2)}\right)^2. \tag{2}$$

The theoretical results for $\frac{C_v}{T^3}$ are plotted as a function of $T$ in figure 5 and compared with the experiment [15]. Since $C_v \approx C_p$ for a solid, we compare directly the calculated $C_v$ with the measurements of $C_p$ (hereafter, $C \equiv C_p = C_v$).

We note that the experimental data (open symbols in figure 5) show an anomalous behaviour at low temperatures, that can be ascribed to the presence of an unknown amount of metallic Mg in the sample used, as already pointed out by Wolf *et al* [15]. Actually, they tried to subtract that contribution from the data, and plotted the final result as $C$ versus $T$. However, this plot does not have the accuracy necessary to ensure the complete elimination of the former contribution. In fact, when these experimental data are plotted as $\frac{C}{T^3}$ versus $T$, we observe that the Mg metallic contribution remains (see figure 5). To correct this behaviour we added a linear contribution of the form $\gamma T$ to the experimental $C$ and fitted the parameter $\gamma$ so that the experimental data of figure 5 extrapolate to the calculated value as $T$ tends to zero. The value of $\gamma$ obtained by this procedure was ≈−0.0077 J $K^{-2}$ $mol^{-1}$.

In figure 5 we show the corrected experimental data with filled square symbols. The position of the maximum for the theoretical curve is at ≈50 K, in good agreement with the experimental corrected data, although the calculated $C$ value is around 35% smaller than the corresponding experimental value. The whole result is quite good considering that the developed model corresponds to a perfect solid. The larger values observed in the experiment compared to our results may be ascribed, on one hand, to the presence of impurity defects

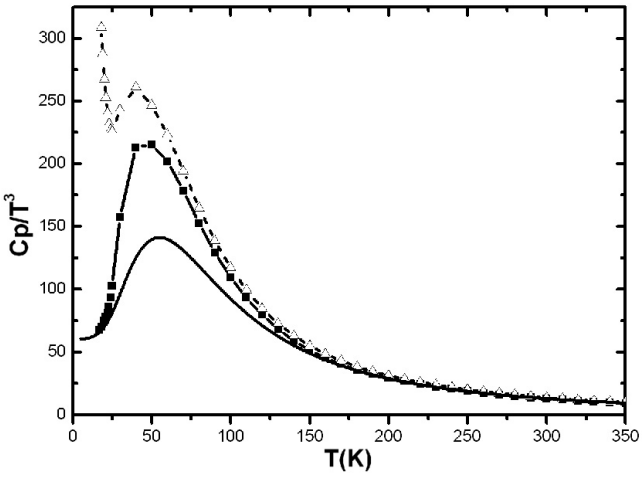


**Figure 5.** Specific heat as a function of temperature. Open triangles and dashed lines indicate the experimental data of [15]; solid squares and solid lines correspond to the same experimental data corrected by a linear term as explained in text. In both cases, lines are only guide to the eye. Solid lines show the results of our SM calculation. The values of $C_p/T^3$ are given in units of $10^{-7}$ J K$^{-4}$ mol$^{-1}$.

and elastic relaxations in the real solid; on the other hand, they may also be ascribed to the uncertainty of the acoustic and low-lying frequency modes of the model, which give the predominant contribution to the specific heat at low temperature.

From the theoretical results of $C$ we have also derived the effective Debye temperature as a function of $T$. The Debye temperature, calculated in the limit $T \to 0$ K, is of the order of 1440 K, which is around 20% lower than the experimental value derived from the reduced moments of the neutron data of [14]. The origin of this difference may be ascribed to an underestimation of the elastic constants derived from our model, related to the slopes of the acoustic dispersion curves as the wavevector tends to zero in figure 2.

The region where the Debye model is strictly valid (Debye region), identified as the region where $\frac{C}{T^3}$ is approximately constant, extends up to $\approx$10 K in our calculation (see figure 5). The low limit of this region is related to the onset of curvature at quite low frequencies in the acoustic dispersion curves, which is a consequence of strong hybridizations between acoustic and low-frequency optical branches towards the Brillouin zone boundary (see figure 2) [16, 17].

## 5. Conclusion

We have presented an *ab initio* calculation of the $\Gamma$ phonons in $MgH_2$ and derived a shell model fitted to the *ab initio* results and the experimental data available from Raman measurements. The frequencies of the *ab initio* $\Gamma$ phonons are in close agreement with the Raman experimental data. The developed shell model gives a very good description of the Raman and silent $\Gamma$ phonons, although some discrepancies arise in comparing the obtained infrared active modes with the first-principles data. The dispersion curves evaluated with our shell model in different symmetry directions of the Brillouin zone are in very good agreement with those derived by a linear response first-principles calculation [6]. By means of the developed shell model, we compute integral properties of the phonon spectrum. The total and projected phonon densities of states give two well defined band regions at low and high energies, corresponding

to Mg and H respectively. These bands are practically unmixed as a consequence of the large mass difference and the ionic nature of the bonding between Mg and H. The small mixture character of the highest energy peaks in the Mg band arises due to hybridizations between the low-frequency optical and acoustic dispersion curves near the Brillouin zone boundary. The calculated partial density of states for hydrogen is in good agreement with data derived from neutron scattering measurements [14]. In particular, the positions and extensions of the main bands, and the gaps and pseudogap between them in the H spectrum, are well reproduced by our calculations. The calculated highest energy peak of the hydrogen PDOS band at $\approx$1470 $cm^{-1}$ was not observed experimentally because neutrons with such energy were not considered [14]. We find that the large widths observed experimentally in the main bands of the hydrogen PDOS data are due to the dispersion of hydrogen optic branches produced by Mg–H interactions and not by H–H interactions, as speculated in [14]. The total DOS obtained by our shell model is also in close agreement with the corresponding magnitude obtained from linear response first-principles calculations [6]. We have also evaluated the specific heat as a function of temperature from the developed shell model in general good agreement with experiment.

## Acknowledgments

This work was supported in part by the Agencia Nacional de Promoción Científica y Tecnológica and CONICET under Grant PICT99 Nr. 03-07248. RM, MS and SK acknowledge additional support from CONICET. SK also thanks Fundación Antorchas, Argentina, for support. We also acknowledge helpful discussions with J Dawidowski.

## References

[1] Jena P and Satterthwaite C B (ed) 1983 *Electronic Structure and Properties of Hydrogen in Metals* (New York: Plenum)
[2] Yu R and Lam P K 1988 *Phys. Rev.* B **37** 8730
[3] Pfrommer B, Elsässer C and Fähnle M 1994 *Phys. Rev.* B **50** 5089
[4] Smithson H, Marianetti C A, Morgan D, Van der Ven A, Predith A and Ceder G 2002 *Phys. Rev.* B **66** 144107
[5] Vajeeston P, Ravindran P, Kjekshus A and Fjellvåg H 2002 *Phys. Rev. Lett.* **89** 175506
[6] Ohba N, Miwa K, Noritake T and Fukumoto A 2004 *Phys. Rev.* B **70** 035102
[7] Blaha P, Schwarz K and Luitz J 1999 *WIEN97, A Full Potential Linearized Augmented Plane Wave Package for Calculating Crystal Properties* (Austria: Karlheinz Schwarz, Techn. Universität Wien) (ISBN 3-9501031-0-4)
[8] Perdew J P, Burke K and Ernzerhof M 1996 *Phys. Rev. Lett.* **77** 3865
[9] Noritake T, Towata S, Aoki M, Seno Y, Hirose Y, Nishibori E, Takata M and Sakata M 2003 *J. Alloys Compounds* **356/357** 84
[10] Ellinger F H, Holley C R, McInteer B B, Pavone D, Potter R M, Staritzsky E and Zachariasen W H 1955 *J. Am. Chem. Soc.* **77** 2647
[11] Katiyar R S 1970 *J. Phys. Chem.* **3** 1087
[12] Mostoller M and Wang J C 1985 *Phys. Rev.* B **32** 6773
[13] Dominguez F A 1998 *Master Thesis* Universidad Nacional de Rosario, Rosario, Argentina, unpublished
[14] Santisteban J R, Cuello G J, Dawidowski J, Fanstein A, Peretti H A, Ivanov A and Bermejo F J 2000 *Phys. Rev.* B **62** 37
[15] Wolf U, Bohmhammel K and Wolf G 1998 *Thermochim. Acta* **310** 37
[16] Koval S, Burriel R, Stachiotti M G, Castro M, Migoni R L, Moreno M S, Varela A and Rodriguez C O 1999 *Phys. Rev.* B **60** 14496
[17] Koval S, Stachiotti M G, Migoni R L, Moreno M S, Mercader R C and Peltzer y Blancá E L 1996 *Phys. Rev.* B **54** 7151